Research Square

Preprints are preliminary reports that have not undergone peer review.
They should not be considered conclusive, used to inform clinical practice,
or referenced by the media as validated information.

Saliva-Based Label-Free Raman Detection of Extracellular Vesicles for Low-Cost Point-of-Care Diagnostics in Resource-Limited Settings

Ajitesh Dhal
Taipei Medical University
Ana Elena Aviña
Taipei Medical University
Cheng-Jen Chang
Taipei Medical University
Pei-Wen Peng
Taipei Medical University
Chih-Yuan Fang
Taipei Medical University
Tzu Sen Yang
tsyang@tmu.edu.tw

Taipei Medical University

Article

Keywords: Extracellular vesicles, Saliva-based diagnostics, Raman spectroscopy, Label-free detection, Point-of-care diagnostics, Low-resource healthcare

Posted Date: May 20th, 2026

DOI: https://doi.org/10.21203/rs.3.rs-9500389/v1

License: This work is licensed under a Creative Commons Attribution 4.0 International License.
Read Full License

Additional Declarations: No competing interests reported.

Saliva-Based Label-Free Raman Detection of Extracellular Vesicles for Low-Cost Point-of-Care Diagnostics in Resource-Limited Settings

Ajitesh Dhal[1,2], Ana Elena Aviña[2,3,4], Cheng-Jen Chang[2,4,5], Pei-Wen Peng[6], Chih-Yuan Fang[7,8], Tzu Sen Yang[1,2,6,9*]

[1]International Ph.D. Program in Biomedical Engineering, College of Biomedical Engineering, Taipei Medical University, New Taipei City 235603, Taiwan. [2] Graduate Institute of Biomedical Optomechatronics, Taipei Medical University, Taipei 110, Taiwan.[3] International PhD Program in Medicine, College of Medicine, Taipei Medical University, Taipei 110, Taiwan. [4] Division of Plastic Surgery, Department of Surgery, Taipei Medical University Hospital, Taipei 110, Taiwan. [5] Department of Surgery, School of Medicine, College of Medicine, Taipei Medical University, Taipei 110, Taiwan. [6] School of Dental Technology, Taipei Medical University, Taipei, Taiwan. [7] School of Dentistry, College of Oral Medicine, Taipei Medical University, Taipei, Taiwan. [8] Division of Oral and Maxillofacial Surgery, Department of Dentistry, Wan Fang Hospital, Taipei Medical University, Taipei, Taiwan. [9] Research Center of Biomedical Device, Taipei Medical University, Taipei 110, Taiwan. email: tsyang@tmu.edu.tw

Saliva-based diagnostics offer a compelling route toward accessible healthcare, particularly in low-resource settings where conventional laboratory infrastructure is limited. Extracellular vesicles (EVs) present in saliva carry molecular signatures reflective of physiological and pathological states, yet their clinical translation is hindered by reliance on complex instrumentation.
Here, we report a label-free Raman spectroscopic approach for rapid biochemical profiling of salivary EVs, integrated with minimally invasive sampling and simplified processing workflows. EVs isolated from human saliva were characterized using cryogenic electron microscopy, nanoparticle tracking analysis, dynamic light scattering, and ExoView, confirming structural integrity and canonical marker expression. Raman spectroscopy enabled acquisition of distinct molecular fingerprints corresponding to proteins, lipids, and nucleic acids without labeling or extensive sample preparation.
Importantly, we outline a pathway toward portable Raman-based detection systems, emphasizing low-cost optics, reduced power requirements, and compatibility with decentralized testing environments. This platform demonstrates the feasibility of non-invasive, rapid, and scalable EV-based diagnostics, supporting the development of point-of-care technologies aimed at improving healthcare accessibility in resource-limited settings.

Keywords: Extracellular vesicles, Saliva-based diagnostics, Raman spectroscopy, Label-free detection, Point-of-care diagnostics, Low-resource healthcare

Extracellular vesicles (EVs) are nanoscale, membrane-bound particles secreted by virtually all cell types and present in a wide range of biological fluids, including blood, urine, and saliva. These vesicles encompass heterogeneous subtypes such as exosomes and microvesicles, which play critical roles in intercellular communication by transporting proteins, lipids, and nucleic acids between cells. [1,2] Importantly, EV cargo reflects the physiological and pathological state of their cells of origin, positioning them as highly informative biomarkers for disease diagnosis, prognosis, and therapeutic monitoring. [3,4]

Among the various biofluids, saliva has emerged as a particularly attractive medium for diagnostic applications. Saliva collection is non-invasive, painless, and does not require specialized personnel or infrastructure, making it especially suitable for decentralized testing environments and large-scale screening programs.[5–7]. In recent years, salivary diagnostics have gained increasing attention for the detection of systemic diseases, including cancer, metabolic disorders, and infectious diseases, highlighting their potential for point-of-care (POC) applications [8–10]. The presence of EVs in saliva further enhances its diagnostic value, as these vesicles provide stable carriers of molecular information protected from enzymatic degradation [11] In addition, recent evidence indicates that the method used to isolate salivary EVs can substantially influence downstream analytical robustness and biomarker detectability, emphasizing the importance of carefully selected and standardized workflows for translational studies. [12]

Despite their promise, current methods for EV characterization remain largely dependent on centralized laboratory infrastructure and specialized equipment. Techniques such as nanoparticle tracking analysis (NTA) and dynamic light scattering (DLS) are widely employed to determine particle size distribution and concentration, while electron microscopy enables direct visualization of vesicle morphology [13,14]. In addition, immunoaffinity-based platforms such as ExoView allow sensitive detection of canonical EV surface markers, including CD9, CD63, and CD81 [15]. More recent advances in EV isolation and detection technologies, including single-vesicle analytical approaches, have further expanded the precision and clinical relevance of EV profiling. [16,17] However, these approaches are often time-consuming, require extensive sample preparation, and rely on costly instrumentation, limiting their applicability in low-resource settings and real-time diagnostic workflows.

Point-of-care diagnostics aim to address these limitations by providing rapid, accessible, and cost-effective testing solutions that can be deployed outside traditional laboratory environments. The World Health Organization has emphasized the importance of ASSURED criteria:Affordable, Sensitive, Specific, User-friendly, Rapid and robust, Equipment-free, and Deliverable to end-users-for diagnostic tools in resource-limited settings [18]. In this context, there is a critical need for analytical platforms that can combine molecular sensitivity with operational simplicity and portability.

Raman spectroscopy is a label-free vibrational spectroscopic technique capable of providing detailed biochemical fingerprints of biological samples through the detection of molecular vibrational modes. It enables simultaneous characterization of proteins, lipids, nucleic acids, and other biomolecules without the need for exogenous labels or extensive sample processing [19,20]. Importantly, Raman spectroscopy offers several advantages for point-of-care applications, including minimal sample preparation, rapid acquisition times, and compatibility with compact and portable instrumentation. [21,22] Recent advances in fiber-optic probes, miniaturized spectrometers, and low-power laser sources have further facilitated the development of Raman-based systems for field-deployable diagnostics [23]. In parallel, recent reviews have highlighted the growing relevance of Raman spectroscopy for EV analysis, including its ability to support biochemical profiling, heterogeneity assessment, and translational diagnostic development. [24]

The integration of Raman spectroscopy with extracellular vesicle analysis represents a promising strategy for non-invasive and rapid diagnostics. Raman-based profiling of

EVs has demonstrated the ability to capture disease-specific molecular signatures, enabling discrimination between physiological and pathological states. [25,26] More recently, computational approaches such as self-supervised learning have further strengthened the capacity of Raman data to identify extracellular vesicles with improved robustness and analytical scalability [27] However, most studies to date have focused on proof-of-concept demonstrations using complex laboratory setups, and translation toward point-of-care applications remains limited.

In this study, we combine saliva-derived extracellular vesicle isolation with label-free Raman spectroscopic analysis to establish a foundation for non-invasive diagnostic platforms. Through multimodal characterization, including cryogenic electron microscopy, nanoparticle tracking analysis, dynamic light scattering, and ExoView profiling, we validate the structural and molecular integrity of salivary EVs. We further demonstrate that Raman spectroscopy can provide rapid biochemical fingerprints of these vesicles, highlighting its potential for integration into portable, low-cost diagnostic systems. This approach supports the development of scalable point-of-care technologies aimed at improving healthcare accessibility, particularly in low-resource settings. Recent work applying Raman spectroscopy specifically to salivary EVs in metabolic disease diagnostics further supports the translational promise of this analytical direction. [28].

Results and Discussion

Multimodal characterization confirms the structural integrity and nanoscale size distribution of salivary extracellular vesicles

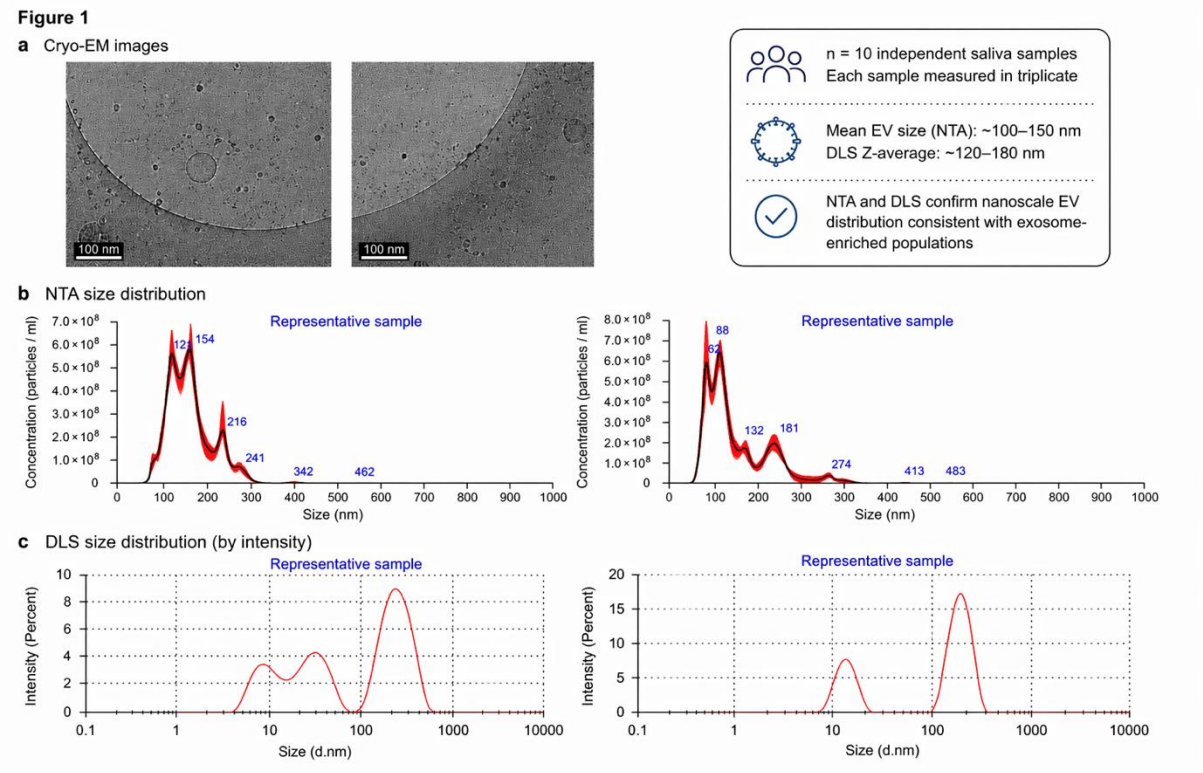

Figure 1. Multimodal characterization of salivary extracellular vesicles. (a) Cryo-EM micrographs show spherical, membrane-bound vesicles with preserved lipid bilayers. Scale bars, 100 nm.(b) NTA size distributions from representative samples (n = 10 donors; triplicates) show a dominant population at ~100–150 nm with minimal larger particles. (c) DLS intensity distributions reveal peaks in the ~100–

200 nm range; Z-average ~100–120 nm with moderate polydispersity. Together, these orthogonal measurements confirm a predominantly small EV population with preserved morphology and consistent nanoscale size.

The presence and structural integrity of extracellular vesicles (EVs) isolated from human saliva were first validated using cryogenic electron microscopy (Cryo-EM). Representative micrographs revealed spherical, membrane-bound vesicles with clearly defined lipid bilayers (Fig. 1a), consistent with canonical EV morphology as described in previous studies [14]. The observed vesicles exhibited diameters within the nanoscale range and lacked signs of aggregation or structural disruption, indicating preservation of vesicular integrity during the isolation process.

To further characterize EV size distribution and concentration, nanoparticle tracking analysis (NTA) was performed. NTA measurements demonstrated that the majority of particles were distributed within the expected EV size range of approximately 50–200 nm, with mean diameters centered around ~100–150 nm (Fig. 1b). These findings are consistent with reported size distributions for exosome-enriched EV populations **(Supplementary Fig. S2)**. [13] The relatively narrow distribution and absence of significant larger particle populations suggest effective removal of cellular debris and larger vesicles during differential centrifugation. This is particularly relevant in salivary EV studies, where isolation methodology can strongly affect particle recovery, purity, and downstream biomarker robustness. [12]

Dynamic light scattering (DLS) analysis provided complementary measurements of hydrodynamic diameter, further confirming the nanoscale size of the isolated vesicles (Fig. 1c). While DLS measurements exhibited slightly broader distributions, as expected due to intensity-weighted analysis, the dominant size populations remained consistent with NTA results **(Supplementary Fig. S1)**. The combined Cryo-EM, NTA, and DLS analyses (Fig. 1) collectively confirm the successful isolation of structurally intact EVs with size distributions characteristic of exosomal populations, in agreement with MISEV2018 guidelines [4] and with current advances in EV isolation and detection workflows. [16]

Table 1. Summary of multimodal characterization of salivary extracellular vesicles

Parameter	Method	Value	Interpretation
Morphology	Cryo-EM	Spherical vesicles with lipid bilayer	Structurally intact EVs
Size (nm)	NTA	~100–150 nm (mode distribution)	Consistent with exosome-enriched population
Size (nm)	DLS	~120–180 nm (hydrodynamic diameter)	Slightly broader distribution due to intensity weighting
Concentration (particles/mL)	NTA	~2.26 × 10^8 particles/mL	Efficient EV isolation yield
CD63 expression (%)	ExoView	~63%	Dominant EV marker population
CD81 expression (%)	ExoView	~23%	Secondary marker population
CD9 expression (%)	ExoView	~13%	Minor EV subpopulation
Marker colocalization	ExoView	Single, double, and triple positive EVs detected	Indicates EV population heterogeneity

Parameter	Method	Value	Interpretation
Nucleic acids (~720 cm^{-1})	Raman spectroscopy	Detected	Presence of RNA/DNA components
Proteins (~1000, ~1650 cm^{-1})	Raman spectroscopy	Detected	Phenylalanine and amide I signatures
Lipids (~1445 cm^{-1})	Raman spectroscopy	Detected	Membrane lipid components

Table 1. Summary of multimodal characterization of salivary extracellular vesicles. Orthogonal techniques including Cryo-EM, NTA, DLS, ExoView, and Raman spectroscopy were used to assess EV morphology, size distribution, concentration, surface marker expression, and biochemical composition. Results are presented as representative values or mean ± SD where applicable. Size measurements by NTA and DLS indicate a predominantly small EV population, while ExoView confirms canonical tetraspanin expression (CD63, CD81, CD9) and population heterogeneity. Raman spectral features corresponding to nucleic acids, proteins, and lipids further validate the molecular composition of isolated EVs.

Surface marker profiling and fluorescence analysis validate EV identity and heterogeneity.

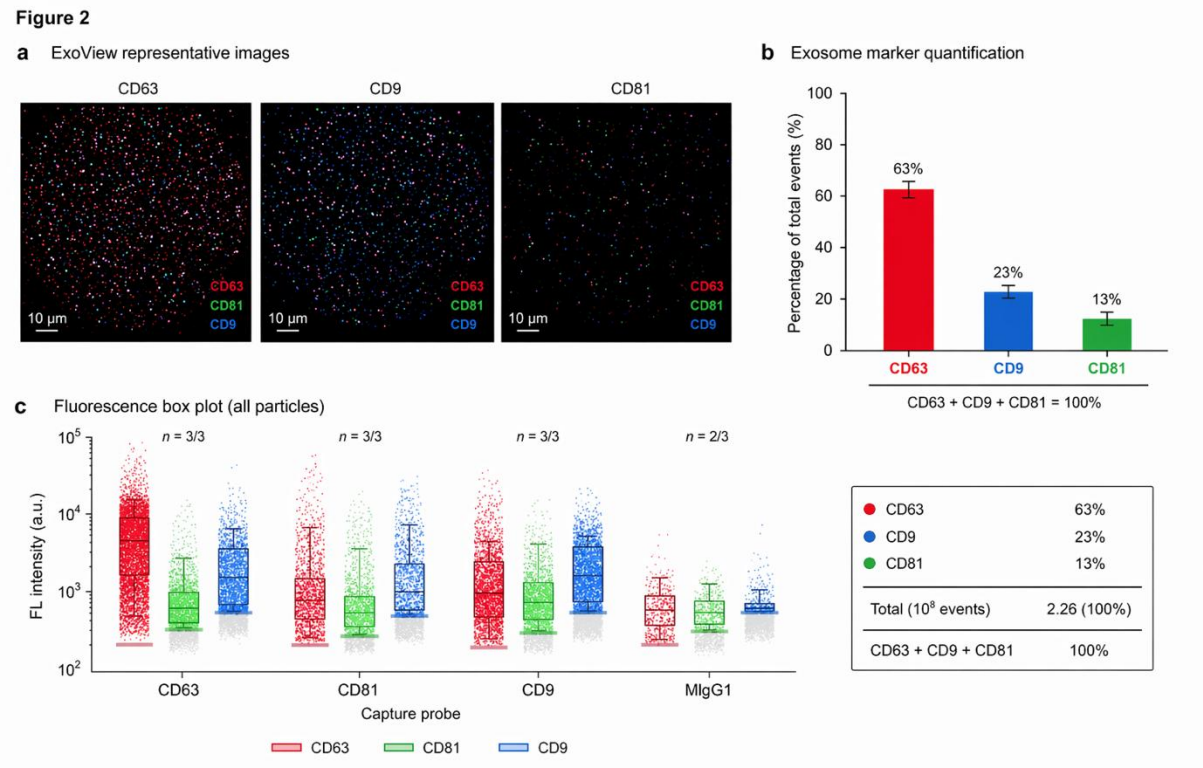

Figure 2. ExoView-based surface marker profiling confirms EV identity and population heterogeneity. (a) Representative ExoView interferometric images of EVs captured via tetraspanin antibodies (CD63, CD9, CD81) show abundant particle binding, with CD63-enriched populations visually predominant. Scale bars, 10 µm.(b) Quantification of marker-positive events demonstrates relative abundance of CD63 (63%), CD9 (23%), and CD81 (13%), with total EV concentration of ~2.26 × 10^8 particles/mL. (c) Fluorescence intensity distributions (all detected particles) across capture probes reveal distinct expression profiles for CD63, CD9, and CD81, with broader signal dispersion for CD63 and CD9 compared to CD81 and minimal signal in IgG control. These data confirm canonical tetraspanin expression and reveal heterogeneous EV subpopulations at the single-vesicle level.

To confirm the molecular identity of the isolated vesicles, ExoView analysis was performed targeting canonical EV tetraspanin markers, including CD63, CD9, and CD81. Interferometric imaging revealed abundant particle binding across all capture antibodies, with CD63-positive vesicles representing the dominant population (Fig. 2a). Quantitative analysis demonstrated that CD63 accounted for the majority of detected EVs, followed by CD81 and CD9, consistent with established EV marker expression profiles. [15]

Fluorescence-based detection further validated marker expression and provided insight into the relative abundance and distribution of EV subpopulations (Fig. 2b). Box plot analysis of fluorescence intensity revealed distinct expression patterns among CD63-, CD81-, and CD9-positive vesicles, reflecting biological heterogeneity within the EV population. Such heterogeneity is a well-recognized feature of EVs and reflects differences in cellular origin, biogenesis pathways, and functional roles. [2] The ability to resolve vesicles at the single-particle level is increasingly recognized as an important step toward clinically informative EV phenotyping. [17]

The integration of interferometric and fluorescence detection confirms the presence of canonical EV surface markers and supports the classification of the isolated particles as bona fide extracellular vesicles **(Supplementary Fig. S3)**. Importantly, the ability to resolve subpopulations based on marker expression highlights the potential of this platform for more refined biomarker analysis in diagnostic applications. Minimal signal in the IgG control further confirms assay specificity **(Supplementary Fig. S4).**

Size distribution and marker colocalization reveal EV population complexity.

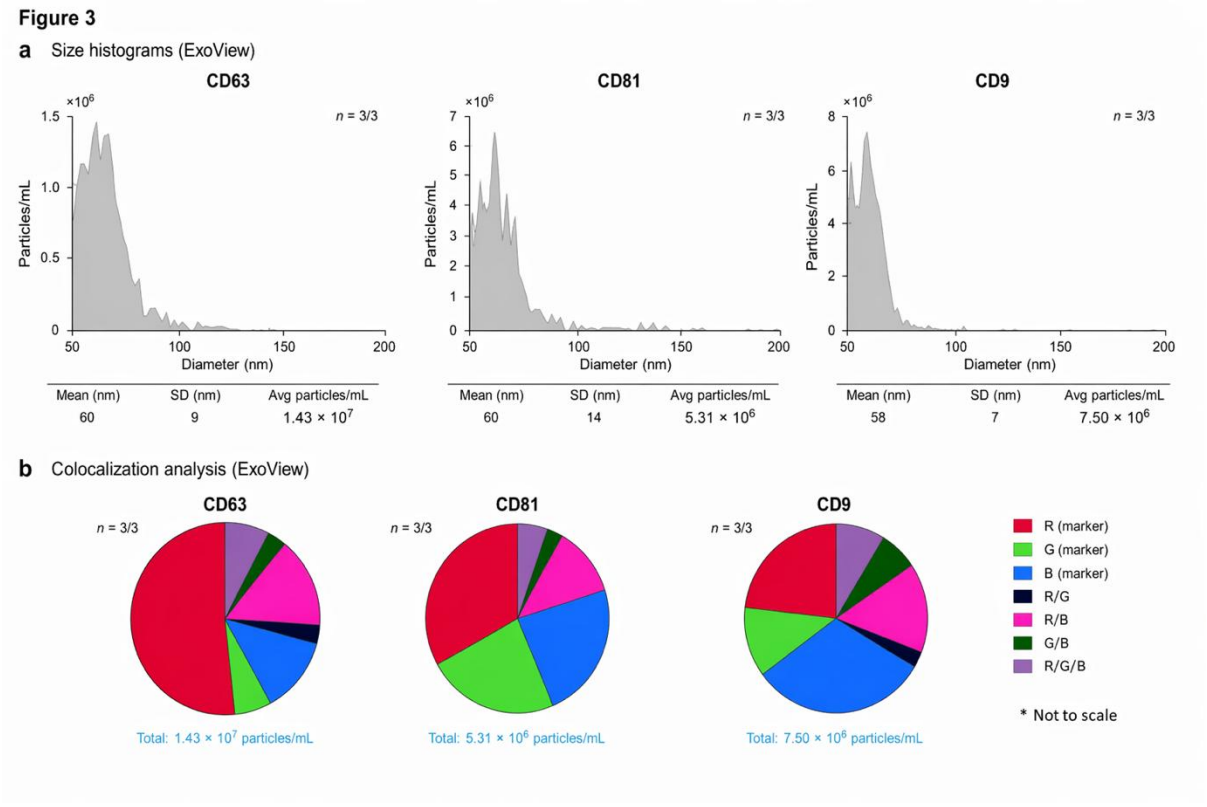

Figure 3. Size distribution and marker colocalization reveal EV population complexity. (a) ExoView-derived size histograms for CD63-, CD81-, and CD9-captured vesicles show particle distributions predominantly within the ~50–100 nm range, with mean diameters of ~60 nm (CD63), ~60 nm (CD81), and ~58 nm (CD9). Particle concentrations vary across markers, reflecting differential capture efficiency

and relative abundance. (b) Colocalization analysis of tetraspanin markers at the single-vesicle level demonstrates heterogeneous EV subpopulations, including single-, double-, and triple-positive events. Pie chart distributions indicate that while single-marker vesicles predominate, a substantial fraction exhibits co-expression of CD63, CD81, and CD9, consistent with the molecular diversity of salivary EVs.T

To further investigate EV population characteristics, size histogram analysis and marker colocalization studies were performed (Fig. 3). Size histograms confirmed that the majority of EVs were distributed within the 50-150 nm range, consistent with NTA and DLS measurements. The relatively narrow distribution suggests a predominance of small EVs, likely corresponding to exosome-enriched fractions.

Colocalization analysis revealed the coexistence of single-, double-, and triple-positive vesicles expressing combinations of CD63, CD9, and CD81 (Fig. 3b). While a significant proportion of vesicles exhibited single-marker expression, a subset displayed co-expression of multiple tetraspanins, reflecting the complex and heterogeneous nature of EV populations. This heterogeneity is consistent with previous reports demonstrating variability in EV marker composition depending on cellular origin and isolation method. [4]

The observed diversity in marker expression and size distribution highlights the importance of multimodal characterization approaches for accurate EV profiling. From a diagnostic perspective, such heterogeneity may provide additional discriminatory power for identifying disease-specific EV signatures.

Raman spectroscopy enables label-free biochemical fingerprinting of salivary EVs

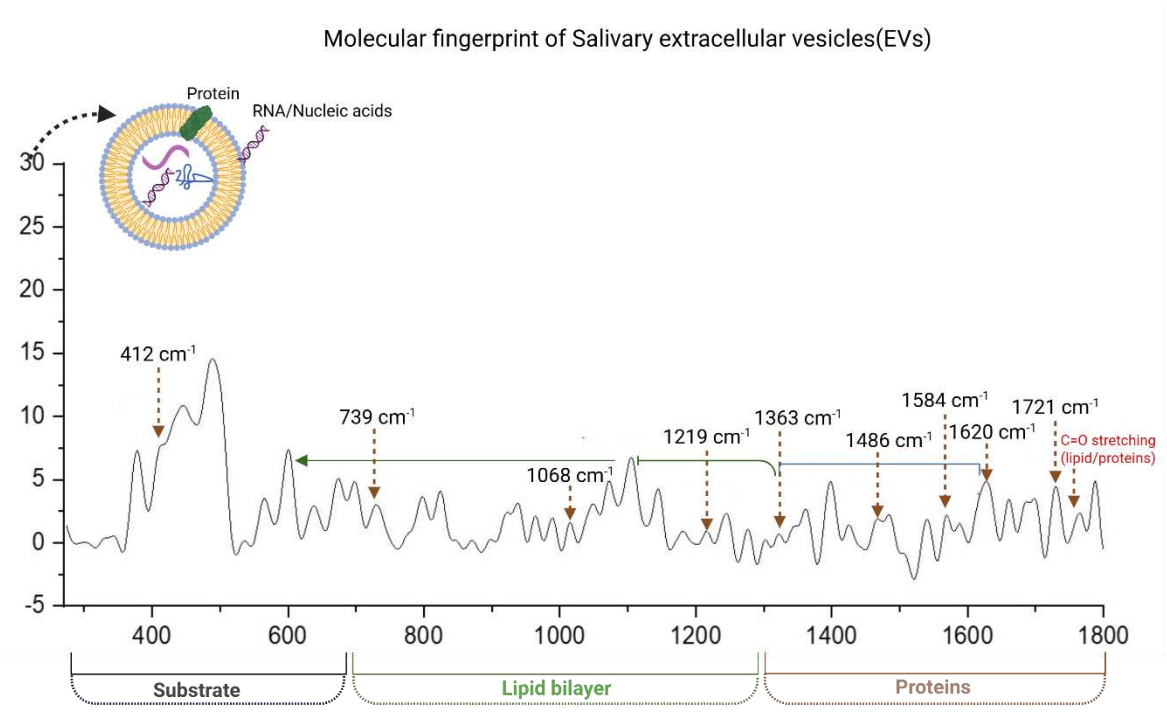

Figure 4. Label-free Raman spectroscopic fingerprint of salivary extracellular vesicles. Representative Raman spectrum of isolated EVs showing distinct vibrational bands corresponding to key biomolecular components. Peaks at ~739 cm^{-1} and ~1068 cm^{-1} are associated with nucleic acids and lipid-related vibrations, while bands at ~1219–1363 cm^{-1} correspond to Amide III and protein-related modes. The

prominent peaks at ~1584 cm^{-1} (Amide II) and ~1620–1721 cm^{-1} (Amide I) indicate protein secondary structure, and the band at ~1486 cm^{-1} reflects CH_2/CH_3 bending from lipids and proteins.

Raman spectroscopic analysis was performed to investigate the biochemical composition of salivary EVs in a label-free manner. The acquired spectra exhibited distinct vibrational bands corresponding to major biomolecular components (Fig. 4). Key spectral features included peaks associated with nucleic acids (~720 cm^{-1}), phenylalanine (~1000 cm^{-1}), lipid CH_2 bending (~1445 cm^{-1}), and protein amide I vibrations (~1650 cm^{-1}), consistent with previously reported Raman signatures of biological materials [19–21]. The simultaneous detection of protein, lipid, and nucleic acid signatures confirms the complex biochemical composition of EVs and supports their role as carriers of molecular information.

Importantly, Raman spectroscopy enabled rapid spectral acquisition without the need for labeling or extensive sample preparation, highlighting its suitability for integration into simplified diagnostic workflows. The ability to capture comprehensive biochemical fingerprints from small sample volumes positions Raman spectroscopy as a powerful tool for EV-based diagnostics. This is consistent with prior demonstrations of Raman-based exosome classification in cancer diagnostics [25] and with recent machine-learning-assisted approaches for EV identification from Raman spectra [27]. In the specific context of saliva-derived EVs, recent evidence also supports the feasibility of combining salivary EV analysis and Raman spectroscopy for precision diagnostics. [28].

Translational potential toward point-of-care diagnostics in low-resource settings

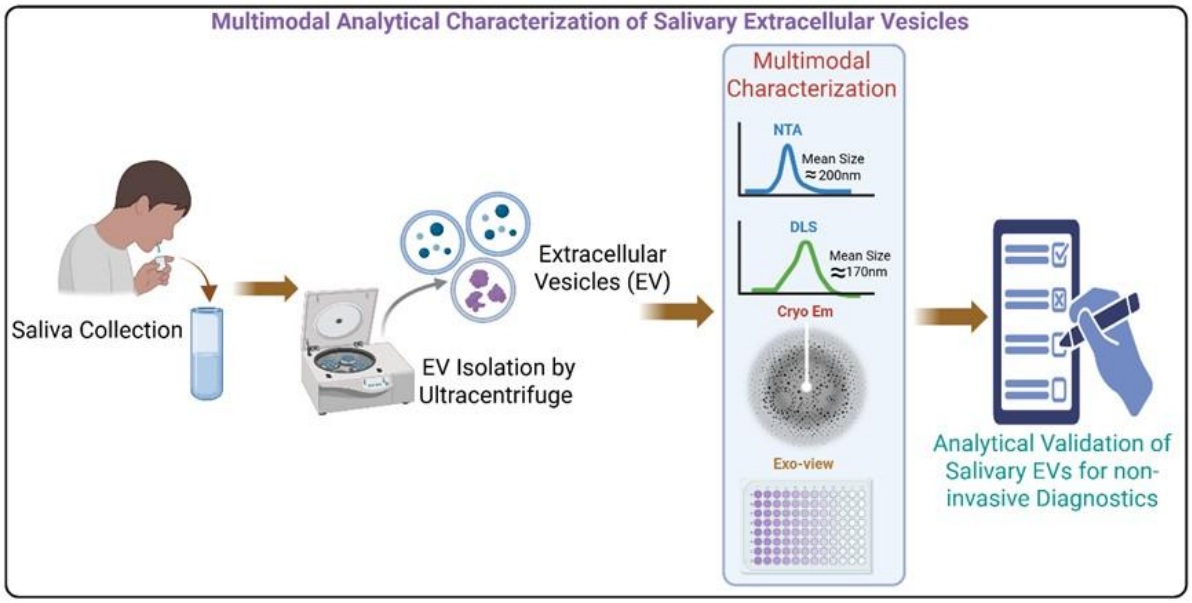

Figure 5. Conceptual framework for saliva-based EV analysis toward point-of-care diagnostics. Schematic overview of the proposed workflow integrating non-invasive saliva collection, EV isolation by ultracentrifugation, and multimodal characterization (NTA, DLS, Cryo-EM, and ExoView) for analytical validation. This streamlined pipeline enables structural, biophysical, and molecular profiling of salivary EVs, forming the basis for label-free diagnostic strategies. The integration of minimal sample preparation, scalable workflows, and compatibility with compact analytical platforms highlights the translational potential of this approach for decentralized, low-cost point-of-care applications in resource-limited settings.

Building upon the multimodal characterization and Raman profiling results, we propose a conceptual framework for translating this approach into point-of-care (POC) diagnostic platforms (Fig. 5). The integration of non-invasive saliva collection, simplified EV isolation, and label-free Raman detection offers several advantages for deployment in resource-limited settings.

First, saliva sampling eliminates the need for invasive procedures and trained personnel, enabling decentralized testing. [5] Second, Raman spectroscopy reduces reliance on reagents and complex sample preparation, aligning with the ASSURED criteria for diagnostics in low-resource environments. [18] Finally, recent advances in portable Raman instrumentation and low-power optical systems support the feasibility of developing compact, field-deployable devices [22]

While further work is required to optimize EV isolation workflows and validate disease-specific signatures, the present study establishes a foundational platform for non-invasive, rapid, and scalable diagnostics. The combination of salivary EV analysis and Raman spectroscopy represents a promising strategy for advancing healthcare accessibility and addressing unmet diagnostic needs in low-resource settings.

Conclusion

This study provides a comprehensive multimodal characterization of salivary extracellular vesicles (EVs) by integrating cryogenic electron microscopy, nanoparticle tracking analysis, dynamic light scattering, and ExoView profiling with label-free Raman spectroscopy. These complementary approaches confirm the structural integrity, nanoscale size distribution, and canonical molecular signatures of salivary EVs, consistent with established extracellular vesicle characterization frameworks.

Notably, Raman spectroscopy enabled rapid, reagent-free biochemical fingerprinting of EVs, capturing key molecular components including proteins, lipids, and nucleic acids within a single measurement. This capability emphasizes its potential as a robust and scalable analytical tool for EV-based diagnostics, particularly in contexts requiring minimal sample preparation and rapid readout.

The integration of non-invasive saliva sampling with label-free spectroscopic detection establishes a promising platform for decentralized diagnostic applications. In alignment with the growing demand for accessible and cost-effective healthcare technologies, this approach offers a viable pathway toward point-of-care diagnostics in low-resource settings. [22]

Future efforts should focus on the integration of simplified EV isolation strategies, miniaturized Raman systems, and advanced spectral analysis for disease-specific classification. Collectively, this work establishes a foundational framework for non-invasive, EV-based diagnostic technologies with the potential to transform accessible healthcare and advance global health equity.

Methods

Ethics statement and saliva collection

All human sample collection procedures were conducted in accordance with relevant institutional guidelines and regulations and approved by TMU-Joint Institutional Review Board (**N202512111**). Written informed consent was obtained from all participants prior to sample collection.

Unstimulated whole saliva samples were collected from healthy adult volunteers into sterile polypropylene tubes, following standardized protocols for salivary diagnostics.[5,6] Participants were instructed to refrain from eating, drinking, smoking, or oral hygiene procedures for at least 1 h prior to sample collection to minimize variability. Samples were collected by passive drool and immediately placed on ice for processing.

Extracellular vesicle isolation

Extracellular vesicles (EVs) were isolated from human saliva using a differential centrifugation and ultracentrifugation strategy conceptually aligned with established protocols for extracellular vesicle recovery from biological fluids and cell culture systems, [29,30] and performed in accordance with the Minimal Information for Studies of Extracellular Vesicles (MISEV2018) guidelines. [4]

Briefly, freshly collected saliva samples were subjected to sequential low- to high-speed centrifugation steps to progressively remove cells, debris, and larger extracellular components. Initial clarification was performed at 300 × g for 10 min at 4 °C to eliminate intact cells, followed by centrifugation at 2,000 × g for 20 min to remove residual cellular debris and large particulates. The resulting supernatant was further centrifuged at 10,000 × g for 30 min to deplete larger vesicles, including microvesicles and apoptotic bodies.

EVs were pelleted by ultracentrifugation at 100,000 × g for 70 min at 4 °C using a fixed-angle rotor, consistent with previously reported high-speed sedimentation approaches [29]. The resulting pellet was washed in sterile (0.1μmfileterd) phosphate-buffered saline (PBS) and subjected to a second ultracentrifugation step under identical conditions to further improve vesicle purity. The final EV pellet was resuspended in sterile PBS and stored at −80 °C until downstream analyses.

All centrifugation procedures were conducted at 4 °C to preserve vesicle integrity and minimize enzymatic degradation. Although the present study utilizes saliva as the source material, the isolation workflow preserves the fundamental principles of sequential sedimentation and ultracentrifugation established for cell-derived EVs, enabling robust recovery of small EV populations while maintaining methodological consistency and reproducibility across biological systems [29,30].

Cryogenic electron microscopy (Cryo-EM)

The morphology and structural integrity of salivary extracellular vesicles (EVs) were examined using cryogenic electron microscopy (Cryo-EM) following established protocols for nanoscale vesicle characterization and preservation of native membrane architecture[12,14].

EV suspensions (3–5 μL) were applied onto glow-discharged holey carbon grids to enhance sample adherence and distribution. Excess liquid was blotted to obtain a thin aqueous film, and samples were rapidly vitrified by plunge-freezing in liquid ethane using a controlled vitrification system, ensuring preservation of vesicles in a near-native hydrated state. All grids were maintained under cryogenic conditions throughout transfer and imaging to prevent ice crystal formation and structural distortion.[31]

Vitrified specimens were examined using a JEOL 2200 FS transmission electron microscope (JEOL, Japan), operated under conditions suitable for high-resolution

nanoscale imaging. Micrographs were acquired at magnifications appropriate for resolving vesicular ultrastructure.
EVs were identified based on their characteristic spherical morphology and lipid bilayer membrane structure. Scale bars were included for size reference.

Nanoparticle tracking analysis (NTA)

Particle size distribution and concentration of EVs were measured using nanoparticle tracking analysis (NTA), enabling single-particle tracking based on Brownian motion. [13]
EV samples were diluted in filtered PBS to achieve optimal particle concentration (typically range of 1×10^7 to 1×10^9 particles/mL) as recommended for accurate particle detection. Measurements were performed using a NanoSight NS300 system (Malvern Panalytical Ltd., UK) equipped with a 532 nm laser and analyzed with NTA software version 3.4 (Malvern Panalytical Ltd.) [29,30]
For each sample, three independent measurements were acquired, with 60 s video recordings per measurement under controlled camera settings. The captured videos were analyzed to calculate particle size distribution, mean and modal diameters, and particle concentration. Distribution percentiles (D10, D50, and D90) were extracted to characterize population heterogeneity.

Dynamic light scattering (DLS)

The hydrodynamic diameter and size distribution of EVs were assessed using dynamic light scattering (DLS), which provides intensity-weighted measurements of particle size [14].
EV suspensions were diluted in PBS and analyzed using a Zetasizer Nano ZS system (Malvern Instruments, UK) operating at a detection wavelength of 633 nm.[29] Measurements were conducted at 25 °C in triplicate to ensure reproducibility.
Data were processed using the instrument's cumulant analysis algorithm to determine the Z-average diameter and polydispersity index (PDI), providing insight into sample homogeneity and aggregation state.

ExoView analysis

Surface marker characterization of EVs was performed using the ExoView R200 platform (NanoView Biosciences, USA), which combines interferometric imaging with fluorescence detection for single-vesicle analysis. [15]
EV samples were incubated on human tetraspanin capture chips functionalized with antibodies against CD63, CD81, and CD9 (Unchained Labs/NanoView Biosciences), within a recommended concentration range of 1×10^7 to 1×10^9 particles/mL as determined by NTA .[29]
Following incubation, chips were washed to remove unbound particles and subsequently labeled with fluorescent detection antibodies. Imaging was performed using the ExoView R200 system in both interferometric and fluorescence modes, with excitation wavelengths of 480 nm, 555 nm, and 640 nm for multiplexed marker detection.
Data were analyzed using ExoView Analyzer software (version 3.2), enabling quantification of particle counts, size distribution, and marker-specific vesicle populations.[29]

Particle counts and marker colocalization were quantified to assess EV identity and heterogeneity.

Fluorescence analysis

Fluorescence intensity data derived from ExoView analysis were used to quantify the relative expression levels of EV surface markers. Signals corresponding to CD63, CD81, and CD9 were extracted from fluorescence channels and analyzed at the single-vesicle level.

Fluorescence intensity distributions were visualized using box plots representing median values, interquartile ranges, and full data dispersion, including outliers. This approach enabled the assessment of population heterogeneity and differential marker expression across EV subpopulations.

Size distribution and colocalization analysis

Size distribution profiles were generated from both NTA and ExoView datasets to characterize EV populations across complementary measurement modalities. Mean diameter and standard deviation were calculated for each capture condition, providing comparative assessment of marker-specific EV size distributions.

Colocalization analysis was performed using ExoView fluorescence data to evaluate the co-expression of canonical tetraspanin markers (CD63, CD81, and CD9) at the single-vesicle level. Vesicles were classified as single-, double-, or triple-positive based on fluorescence signal overlap across channels.

The relative proportions of each subpopulation were quantified and graphically represented, enabling detailed characterization of EV heterogeneity and supporting the identification of distinct vesicle subsets with potential biological and diagnostic relevance.

Raman spectroscopy

Raman spectroscopic analysis was performed to obtain label-free biochemical fingerprints of salivary EVs [19–22].

Raman spectra were acquired using a Raman tweezers system configured as previously described. [32] The platform consisted of an inverted microscope (TE2000-S, Nikon Corporation, Tokyo, Japan) equipped with a 60× oil-immersion objective (NA 1.4, Nikon, Tokyo, Japan), an in-house motorized X-Y translation stage, and a 785 nm diode laser delivering ~11 mW at the sample. Raman signals were collected using an Andor Shamrock 193i spectrometer with a 600 lines/mm grating and detected with an iVac 316 CCD cooled to −75 °C. A Hamamatsu C13440-20CU CMOS camera and an Andor LucaEM S658M EMCCD camera were used for sample visualization and alignment. [32]

Isolated salivary EVs suspended in PBS were subjected to label-free Raman analysis. Spectra were collected over the 333–1800 cm^{-1} region, encompassing the principal fingerprint bands of biologically relevant macromolecules. Background spectra recorded from particle-free areas were subtracted from each acquisition, and measurements were performed under minimized ambient light conditions.

Raman bands were interpreted using established assignments for nucleic acids, proteins, and lipids in biological samples and extracellular vesicles. [19,20,24]

Statistical analysis

All measurements were performed in at least three independent experiments unless otherwise stated. Data are presented as mean ± standard deviation (SD) or standard error of the mean (SEM), as indicated.
Statistical analyses were conducted using GraphPad Prism version 8.0.1 (GraphPad Software, Inc., San Diego, CA, USA). A p-value < 0.05 was considered statistically significant.

Data availability.

All data generated or analysed during this study are included in this published article and its Supplementary Information files. Additional details supporting the findings of this study are available from the corresponding author upon reasonable request.

References

1. Raposo, G. & Stoorvogel, W. Extracellular vesicles: Exosomes, microvesicles, and friends. *Journal of Cell Biology* **200**, 373–383 (2013).
2. Yáñez-Mó, M. *et al.* Biological properties of extracellular vesicles and their physiological functions. *J of Extracellular Vesicle* **4**, 27066 (2015).
3. Valadi, H. *et al.* Exosome-mediated transfer of mRNAs and microRNAs is a novel mechanism of genetic exchange between cells. *Nat Cell Biol* **9**, 654–659 (2007).
4. Théry, C. *et al.* Minimal information for studies of extracellular vesicles 2018 (MISEV2018): a position statement of the International Society for Extracellular Vesicles and update of the MISEV2014 guidelines. *J of Extracellular Vesicle* **7**, 1535750 (2018).
5. Lee, Y.-H. & Wong, D. T. Saliva: an emerging biofluid for early detection of diseases. *Am J Dent* **22**, 241–248 (2009).
6. Zhang, C.-Z. *et al.* Saliva in the diagnosis of diseases. *Int J Oral Sci* **8**, 133–137 (2016).
7. Zhang, L., Xiao, H. & Wong, D. T. Salivary Biomarkers for Clinical Applications. *Mol Diag Ther* **13**, 245–259 (2009).
8. Malon, R. S. P., Sadir, S., Balakrishnan, M. & Córcoles, E. P. Saliva-Based Biosensors: Noninvasive Monitoring Tool for Clinical Diagnostics. *BioMed Research International* **2014**, 1–20 (2014).
9. Cuevas-Córdoba, B. & Santiago-García, J. Saliva: A Fluid of Study for OMICS. *OMICS: A Journal of Integrative Biology* **18**, 87–97 (2014).
10. Carney, R. P., Navas-Moreno, M. & Birkeland, A. Abstract 1067: Label free Raman spectroscopy of extracellular vesicles for early stage liquid biopsy cancer detection. *Cancer Research* **84**, 1067–1067 (2024).
11. Michael, A. *et al.* Exosomes from human saliva as a source of microRNA biomarkers: microRNA biomarkers in salivary exosomes. *Oral Diseases* **16**, 34–38 (2010).
12. Boulestreau, J. *et al.* Salivary extracellular vesicles isolation methods impact the robustness of downstream biomarkers detection. *Sci Rep* **14**, 31233 (2024).
13. Dragovic, R. A. *et al.* Sizing and phenotyping of cellular vesicles using Nanoparticle Tracking Analysis. *Nanomedicine: Nanotechnology, Biology and Medicine* **7**, 780–788 (2011).

14. Arraud, N. *et al.* Extracellular vesicles from blood plasma: determination of their morphology, size, phenotype and concentration. *Journal of Thrombosis and Haemostasis* **12**, 614–627 (2014).
15. Daaboul, G. G. *et al.* Digital Detection of Exosomes by Interferometric Imaging. *Sci Rep* **6**, 37246 (2016).
16. Li, B., Wu, W., Xu, W., Qian, H. & Ji, C. Advances of extracellular vesicles isolation and detection frontier technology: from heterogeneity analysis to clinical application. *J Nanobiotechnol* **23**, 678 (2025).
17. Tran, H. L. *et al.* Extracellular Vesicles for Clinical Diagnostics: From Bulk Measurements to Single-Vesicle Analysis. *ACS Nano* **19**, 28021–28109 (2025).
18. Peeling, R. W., Holmes, K. K., Mabey, D. & Ronald, A. Rapid tests for sexually transmitted infections (STIs): the way forward. *Sexually Transmitted Infections* **82**, v1–v6 (2006).
19. Movasaghi, Z., Rehman, S. & Rehman, I. U. Raman Spectroscopy of Biological Tissues. *Applied Spectroscopy Reviews* **42**, 493–541 (2007).
20. Butler, H. J. *et al.* Using Raman spectroscopy to characterize biological materials. *Nat Protoc* **11**, 664–687 (2016).
21. Krafft, C., Schie, I. W., Meyer, T., Schmitt, M. & Popp, J. Developments in spontaneous and coherent Raman scattering microscopic imaging for biomedical applications. *Chem. Soc. Rev.* **45**, 1819–1849 (2016).
22. Pilot, R. *et al.* A Review on Surface-Enhanced Raman Scattering. *Biosensors* **9**, 57 (2019).
23. Pahlow, S. *et al.* Isolation and identification of bacteria by means of Raman spectroscopy. *Advanced Drug Delivery Reviews* **89**, 105–120 (2015).
24. Liu, Y.-J., Kyne, M., Kang, C. & Wang, C. Raman spectroscopy in extracellular vesicles analysis: Techniques, applications and advancements. *Biosensors and Bioelectronics* **270**, 116970 (2025).
25. Shin, H. *et al.* Early-Stage Lung Cancer Diagnosis by Deep Learning-Based Spectroscopic Analysis of Circulating Exosomes. *ACS Nano* **14**, 5435–5444 (2020).
26. Shin, H. *et al.* Single test-based diagnosis of multiple cancer types using Exosome-SERS-AI for early stage cancers. *Nat Commun* **14**, 1644 (2023).
27. Jensen, M. N. *et al.* Identification of extracellular vesicles from their Raman spectra via self-supervised learning. *Sci Rep* **14**, 6791 (2024).
28. Dhal, A. *et al.* Salivary extracellular vesicles and Raman spectroscopy in precision diagnostics of type 2 diabetes. *Diabetes Research and Clinical Practice* **233**, 113139 (2026).
29. Chang, C.-Y. *et al.* Exploring the biphasic dose-response effects of photobiomodulation on the viability, migration, and extracellular vesicle secretion of human adipose mesenchymal stem cells. *Journal of Photochemistry and Photobiology B: Biology* **256**, 112940 (2024).
30. Hang, N. L. T. *et al.* Photobiomodulation associated with alginate-based engineered tissue on promoting chondrocytes-derived biological responses for cartilage regeneration. *International Journal of Biological Macromolecules* **280**, 135982 (2024).
31. Linares, R., Tan, S., Gounou, C. & Brisson, A. R. Imaging and Quantification of Extracellular Vesicles by Transmission Electron Microscopy. in *Exosomes and Microvesicles* (ed. Hill, A. F.) vol. 1545 43–54 (Springer New York, New York, NY, 2017).

32. Hien, N. D. *et al.* Integration of Raman tweezers and machine learning for label-free single-cell characterization of endometriosis cells. *Analyst* **151**, 1948–1959 (2026).

Acknowlegements.

The authors gratefully acknowledge the Center for Academic Literacy at National Taiwan Normal University for assistance with English editing of the manuscript, as well as the members of the Biophotonics Laboratory at Taipei Medical University for their technical support and valuable discussions.

Author contributions.

Conceptualization, A.D., A.E.A., C.-J.C. and T.-S.Y.; methodology, A.D., A.E.A., P.-W.P., C.-Y.F. and T.-S.Y.; investigation, A.D., P.-W.P. and C.-Y.F.; data curation, A.D. and A.E.A.; formal analysis and data interpretation, A.D., A.E.A. and C.-Y.F.; visualization, A.D. and A.E.A.; resources, C.-J.C. and T.-S.Y.; writing-original draft preparation, A.D. and A.E.A.; writing-review and editing, A.E.A., C.-J.C. and T.-S.Y.; supervision, C.-J.C. and T.-S.Y.; project administration, C.-J.C. and T.-S.Y.; funding acquisition, C.-J.C. and T.-S.Y.

Funding

This research was supported by the Ministry of Education, Taiwan (grant numbers OGE-UAATUTS-NTUST-114-001) and the National Science and Technology Council (NSTC), Taiwan (grant number NSTC 114-2221-E-038-006).

Declarations.

Competing interests.
The authors declare no competing interests.

Additional information
Supplementary Information The online version contains supplementary material available at

Correspondence and requests for materials should be addressed to T.-S.Y.

Figure Legends

Figure 1. Multimodal characterization of salivary extracellular vesicles. (a) Cryo-EM micrographs show spherical, membrane-bound vesicles with preserved lipid bilayers. Scale bars, 100 nm.(b) NTA size distributions from representative samples (n = 10 donors; triplicates) show a dominant population at ~100–150 nm with minimal larger particles. (c) DLS intensity distributions reveal peaks in the ~100–200 nm range; Z-average ~100–120 nm with moderate polydispersity. Together, these orthogonal measurements confirm a predominantly small EV population with preserved morphology and consistent nanoscale size.

Figure 2. ExoView-based surface marker profiling confirms EV identity and population heterogeneity. (a) Representative ExoView interferometric images of EVs captured via tetraspanin antibodies (CD63, CD9, CD81) show abundant particle binding, with CD63-enriched populations visually predominant.

Scale bars, 10 μm.(b) Quantification of marker-positive events demonstrates relative abundance of CD63 (63%), CD9 (23%), and CD81 (13%), with total EV concentration of ~2.26 × 10^8 particles/mL. (c) Fluorescence intensity distributions (all detected particles) across capture probes reveal distinct expression profiles for CD63, CD9, and CD81, with broader signal dispersion for CD63 and CD9 compared to CD81 and minimal signal in IgG control. These data confirm canonical tetraspanin expression and reveal heterogeneous EV subpopulations at the single-vesicle level.

Figure 3. Size distribution and marker colocalization reveal EV population complexity. (a) ExoView-derived size histograms for CD63-, CD81-, and CD9-captured vesicles show particle distributions predominantly within the ~50–100 nm range, with mean diameters of ~60 nm (CD63), ~60 nm (CD81), and ~58 nm (CD9). Particle concentrations vary across markers, reflecting differential capture efficiency and relative abundance. (b) Colocalization analysis of tetraspanin markers at the single-vesicle level demonstrates heterogeneous EV subpopulations, including single-, double-, and triple-positive events. Pie chart distributions indicate that while single-marker vesicles predominate, a substantial fraction exhibits co-expression of CD63, CD81, and CD9, consistent with the molecular diversity of salivary EVs.T

Figure 4. Label-free Raman spectroscopic fingerprint of salivary extracellular vesicles. Representative Raman spectrum of isolated EVs showing distinct vibrational bands corresponding to key biomolecular components. Peaks at ~739 cm^{-1} and ~1068 cm^{-1} are associated with nucleic acids and lipid-related vibrations, while bands at ~1219–1363 cm^{-1} correspond to Amide III and protein-related modes. The prominent peaks at ~1584 cm^{-1} (Amide II) and ~1620–1721 cm^{-1} (Amide I) indicate protein secondary structure, and the band at ~1486 cm^{-1} reflects CH_2/CH_3 bending from lipids and proteins.

Figure 5. Conceptual framework for saliva-based EV analysis toward point-of-care diagnostics. Schematic overview of the proposed workflow integrating non-invasive saliva collection, EV isolation by ultracentrifugation, and multimodal characterization (NTA, DLS, Cryo-EM, and ExoView) for analytical validation. This streamlined pipeline enables structural, biophysical, and molecular profiling of salivary EVs, forming the basis for label-free diagnostic strategies. The integration of minimal sample preparation, scalable workflows, and compatibility with compact analytical platforms highlights the translational potential of this approach for decentralized, low-cost point-of-care applications in resource-limited settings.

Tables

Table 1. Summary of multimodal characterization of salivary extracellular vesicles

Parameter	Method	Value	Interpretation
Morphology	Cryo-EM	Spherical vesicles with lipid bilayer	Structurally intact EVs
Size (nm)	NTA	~100–150 nm (mode distribution)	Consistent with exosome-enriched population
Size (nm)	DLS	~120–180 nm (hydrodynamic diameter)	Slightly broader distribution due to intensity weighting
Concentration (particles/mL)	NTA	~2.26 × 10^8 particles/mL	Efficient EV isolation yield
CD63 expression (%)	ExoView	~63%	Dominant EV marker population
CD81 expression (%)	ExoView	~23%	Secondary marker population
CD9 expression (%)	ExoView	~13%	Minor EV subpopulation
Marker colocalization	ExoView	Single, double, and triple positive EVs detected	Indicates EV population heterogeneity
Nucleic acids (~720 cm^{-1})	Raman spectroscopy	Detected	Presence of RNA/DNA components

Parameter	Method	Value	Interpretation
Proteins (~1000, ~1650 cm^{-1})	Raman spectroscopy	Detected	Phenylalanine and amide I signatures
Lipids (~1445 cm^{-1})	Raman spectroscopy	Detected	Membrane lipid components

Table 1. Summary of multimodal characterization of salivary extracellular vesicles. Orthogonal techniques including Cryo-EM, NTA, DLS, ExoView, and Raman spectroscopy were used to assess EV morphology, size distribution, concentration, surface marker expression, and biochemical composition. Results are presented as representative values or mean ± SD where applicable. Size measurements by NTA and DLS indicate a predominantly small EV population, while ExoView confirms canonical tetraspanin expression (CD63, CD81, CD9) and population heterogeneity. Raman spectral features corresponding to nucleic acids, proteins, and lipids further validate the molecular composition of isolated EVs.

Supplementary Files

This is a list of supplementary files associated with this preprint. Click to download.

- SupplementaryInformation.pdf